First publ. in: Materials Research Society Symposium V, 866 (2005)

Rare earth ion implantation for silicon based light emission: From infrared to ultraviolet

W. Skorupa[1,2], J. M. Sun[1], S.Prucnal[1], L.Rebohle[2], T. Gebel[2], A.N. Nazarov[3], I.N. Osiyuk[3], T. Dekorsy[1], and M. Helm[1,2]

[1] Forschungszentrum Rossendorf, Institute of Ion Beam Physics and Materials Research, POB 510119, D-01314 Dresden, Germany
[2]nanoparc GmbH, Dresden - Rossendorf, Germany
[3] Institute of Semiconductor Physics, National Academy of Sciences of Ukraine, Kyiv, Ukraine

corresponding author: w.skorupa@fz-rossendorf.de

ABSTRACT

Using ion implantation different rare earth luminescent centers (Gd^{3+}, Tb^{3+}, Eu^{3+}, Ce^{3+}, Tm^{3+}, Er^{3+}) were incorporated into the silicon dioxide layer of a purpose-designed Metal Oxide Silicon (MOS) capacitor with advanced electrical performance, further called a MOS-light emitting device (MOSLED). The silicon dioxide layer did not contain silicon nanoclusters. Efficient electroluminescence was obtained from UV to infrared with a transparent top electrode made of indium-tin oxide. The electroluminescence properties were studied with respect to the luminescence spectra, decay time, impact excitation, cross relaxation (Tb^{3+}), and power efficiency. Top values of the efficiency of 0.3 % corresponding to external quantum efficiencies well above the percent range were reached. The electrical properties of these devices such as current-voltage and charge trapping characteristics, were also evaluated. Moreover, we demonstrate photo- and electroluminescence in correlation to charge trapping characteristics for Er-rich MOSLEDs with a varying silicon cluster content. Finally, application aspects to the field of biosensing will be discussed.

1. INTRODUCTION

Combining silicon-based electronic circuits with optoelectronic functionality is one of the key challenges for the future semiconductor technology. As the packaging density of transistors becomes higher and higher in the ultra-large-scale integrated (ULSI) circuits, the problems of overheating and signal delay become serious from an increase of metallic interconnects. One possible solution could be optical interconnects integrated with silicon technology. The implementation of silicon-based optical interconnection requires light emitters, waveguides, modulators, and photodetectors. Unfortunately, silicon is badly suited to operate as a light emitter due to its indirect band gap of about 1.1 eV. During the last 15 years an enormous research and development activity started throughout the international scene. In this framework it was successfully demonstrated that ion beam processing of silicon and silicon dioxide can lead to convincing solutions regarding silicon based light emission. There exist already numerous articles reviewing the state of the art of light emitters based on silicon-silicon dioxide technology. The reader is kindly referred to the proceedings of the recent Workshop on „Towards the First Silicon Laser“ by Pavesi et al. [1] and references therein to get a satisfactory review of the topic.

In this paper recent work regarding rare earth (RE) implanted light emitters performed as part of the research undertaken by Forschungszentrum Rossendorf and nanoparc GmbH will be

shortly reviewed. This is based on the recent development of a reliable MOSLED containing a light emitting Ge-rich silicon dioxide layer [2,3].

DEVICE PREPARATION

Samples were prepared by the complementary metal-oxide-semiconductor technology on 4-inch, {100} oriented, n-type silicon wafer with resistivity of 2-5 Ω·cm. The MOSLEDs were fabricated by local oxidation of silicon (LOCOS) with a field oxide thickness of one µm. The active layer was a 100 nm thick thermally grown SiO_2 layer implanted with RE^+ ions (Gd^{3+}, Tb^{3+}, Eu^{3+}, Ce^{3+}, Tm^{3+}, Er^{3+}) at two energies of 50 and 110 keV. The implantation doses were adjusted to generate a nearly constant RE concentration in a depth from 27 to 55 nm below the surface of the active layer. The profile of as implanted RE atoms with doses of 1.5E15cm^{-2} at 50 keV and 3E15cm^{-2} at 110keV calculated by TRIM 98 shows a RE concentration of 1.5%, as confirmed by Rutherford backscattering spectrometry (RBS). The atomic concentration was varied from 0.05 to 3 % for different RE's. After implantation, the samples were furnace annealed at 800°C-1100°C in flowing N_2 for 1 hour. The gate electrode was a 100 nm transparent indium-tin-oxide layer deposited by RF sputtering. Various shapes of MOSLEDs with different feature sizes in the range from 0.5 to 500 µm were fabricated for testing the function of the devices in dependence on the geometry.

ELECTROLUMINESCENCE FROM RE-DOPED MOSLEDs

EL spectra were measured on a MOS structure with a circular ITO electrode (diameter: 500 µm) at a constant current supplied by a Keithley 2410 sourcemeter. EL was observed at both positive and negative polarities of the applied voltage. The measurement was normally done with electron injection from the Si substrate into the RE-doped SiO_2. The EL signal was recorded at room temperature with a monochromator (JOBIN YVON Triax 320) and a photomultiplier (Hamamatsu H7732-10). The EL intensity, the injection current and the applied voltage were simultaneously recorded with a multiple channel data acquisition system. The absolute EL power from the device was measured using a calibrated optical power meter (Newport 818-SL). The external EL power efficiency was calculated by integrating the total EL output power from the front surface of the devices and dividing by the total input electric power. PL and PL excitation (PLE) spectra, when necessary, were also measured with the same system using a 75 W xenon lamp as an ultraviolet light source. The EL decay time was measured under the excitation of 100 µs voltage pulses by a multi-channel scaler (Stanford Research System SR430). The minimum time resolution of the system is 10 ns.

In Fig. 1 an overview of the measured EL spectra in the visible wavelength range (except for Er) is shown. From the maximum intensity numbers (see caption) it is obvious that Tb and Gd deliver up to now the most promising emitters except the well reported luminescence of Er in the IR range (not shown). Using the $^6P_{7/2}$ to $^8S_{7/2}$ transition of the Gd^{3+} ion we demonstrated recently the first Si-based light emitter in the UV range with a wavelength of 316 nm and an external quantum efficiency of 1 % [4]. In the following we will report the analysis of the Tb-related electroluminescence in more detail, see also Ref. [5]. Thereafter we will refer to recent work on the electrical performance of Er implanted SiO_2 layers with varying Si-cluster content.

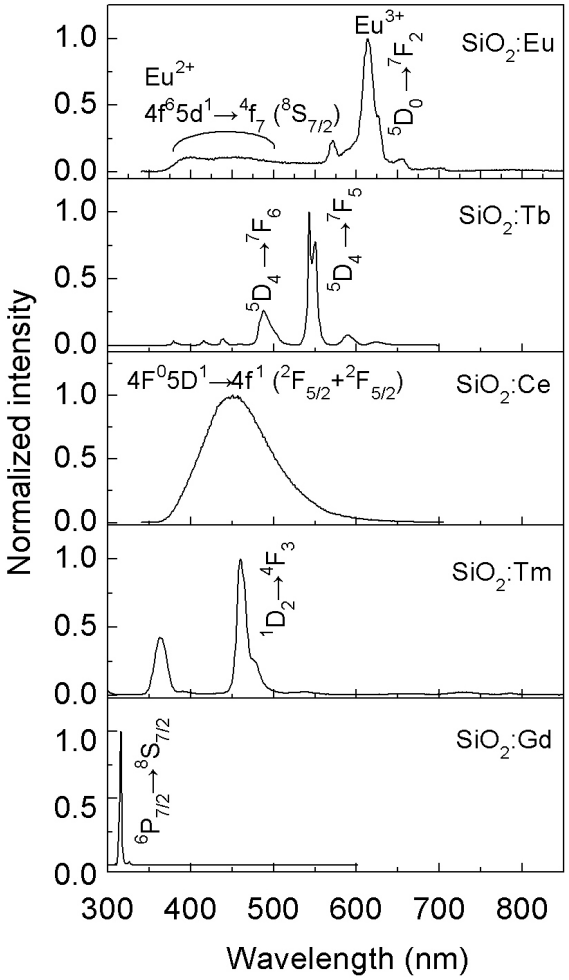

Figure 1. Overview of EL spectra in the visible range of different RE-elements embedded in a MOSLED. The maximum EL intensity values for the strongest peak are: 40647 for Tb^{3+}, 18987 for Gd^{3+}, 1746 for Ce^{3+}, 882 for Tm^{3+}, 457 for Eu^{3+}, and 1.5 for unimplanted SiO_2 (not shown).

Tb-BASED GREEEN ELECTROLUMINESCENCE

EL and current-field characteristics

Fig.2 shows the electronic transitions and the normalized EL spectra from different MOSLEDs with a 100 nm SiO_2:Tb^{3+} active layer and different Tb concentrations of 0.05, 0.15, 0.5 and 1.5 %. The spectra were normalized to the same peak amplitude of the 541 nm line. All samples were annealed at 800°C for 1h. The spectra show two groups of peaks regarding the $^5D_3$ and $^5D_4$ to ^7F_j (j=3-6) transitions of Tb atoms. The relative peak intensity of the $^5D_3$ to ^7F_j (j=3-6) transitions decreases with increasing Tb^{3+} concentration as distinct from that of the $^5D_4$ to ^7F_j transitions remaining constant. Fig.3 (a) shows the current-electric field characteristics for devices with different Tb concentration of 0.15, 0.5, 1.5, and 3 %. The current-field characteristic of the unimplanted SiO_2 is also shown for comparison. At a low average electric field below 8 MV/cm, the small injection current is mainly driven due to the tunneling of

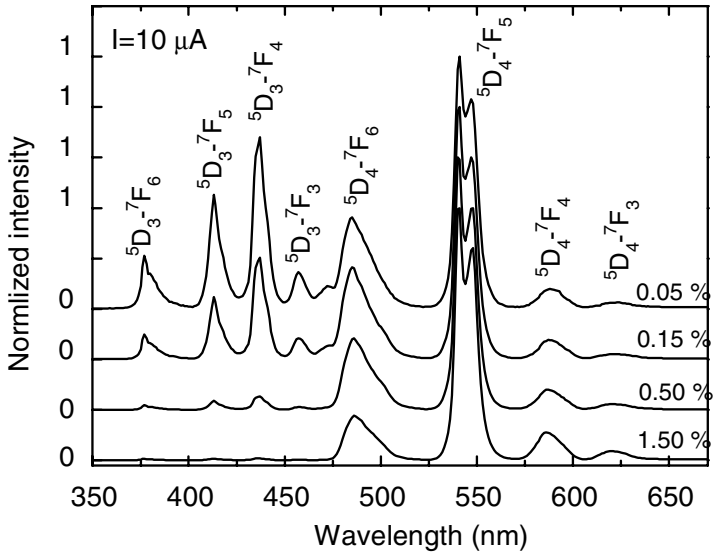

Figure 2. EL spectra of Tb^{3+} ions in MOSLEDs with different Tb concentrations and the related electronic transitions. All spectra are measured at a constant injection current of 10 μA and are normalized relative to the peak intensity of the $^5D_4$-$^7F_5$ transitions at 541 nm.

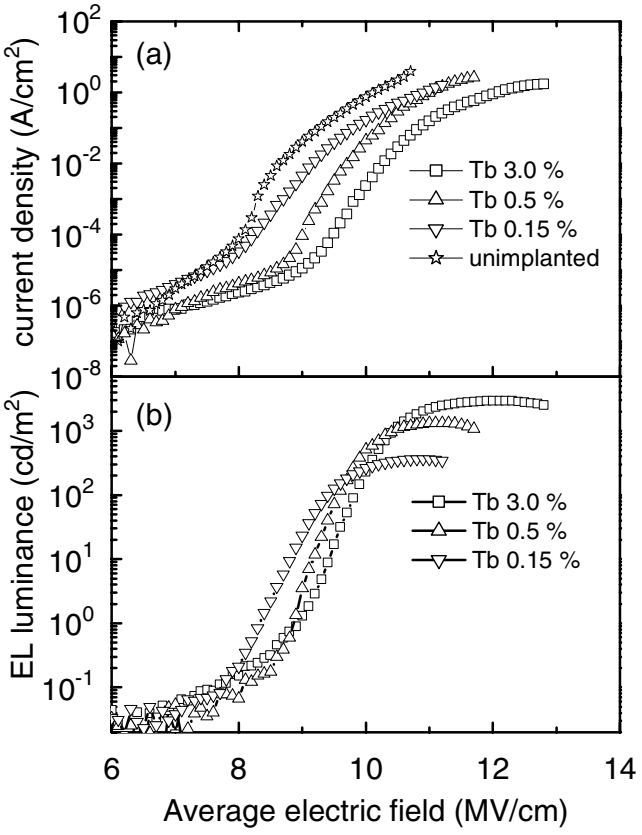

Figure 3(a). Current density versus electric field (J-E) characteristics for MOSLEDs with different Tb concentrations of 0.15, 0.5, and 3 %. The unimplanted thermally grown SiO_2 sample is also shown for comparison. **(b)** Dependence of the EL luminance on the average electric field for the same Tb-doped devices.

electrons between the residual defects in the oxide layers. An onset of strong current injection is observed by increasing the electric field above 8-9 MV/cm. The strong current injection is verified as Fowler-Nordheim (F-N) tunneling injection of electrons from the silicon substrate via the Si/SiO_2 interface. At higher currents the current-field characteristics changes to a linear regime due to the series resistance of the device structure. The threshold electric field for the F-N tunneling shifts slightly from 8 to 9 MV/cm with increasing Tb concentration. This is probably caused by a shift of the flat band voltage of the MOS device due to increased electron trapping as deduced from capacitance-voltage (C-V) measurements (see chapter on charge trapping). Fig.3 (b) shows the dependence of the EL brightness of the green peak at 541 nm on the average electric field for devices with different Tb concentration. The onset of the strong EL emission is correlated with the strong current injection above 8 MV/cm. This indicates that the excitation of EL from Tb is correlated to Fowler-Nordheim (F-N) tunneling injection of hot electrons from the silicon substrate to the conduction band of SiO_2. Top values of the EL luminance of up to 2800 cd/m^2 were achieved for a Tb concentration of 3 % at a current density above 10^{-1} A/cm^2.

Fig.4 demonstrates the dependency of the EL power efficiency and the external quantum efficiency on the Tb concentration for samples annealed at 800°C and 900°C. A decrease in the EL efficiency is observed at the higher annealing temperature of 900°C for samples with a Tb concentration above 0.5 %. The EL efficiency increases linearly with increasing Tb concentration and then saturates above 2 % due to the concentration quenching effect. A high power efficiency of 0.3 % (corresponding to a quantum efficiency of 16 % and luminous efficiency of 2.1 lm/W) is obtained for devices with a Tb concentration of 3 %. The quantum efficiency of our devices is comparable to those commercial green light emitting diodes based on InGaN quantum wells (16.5% [6])!

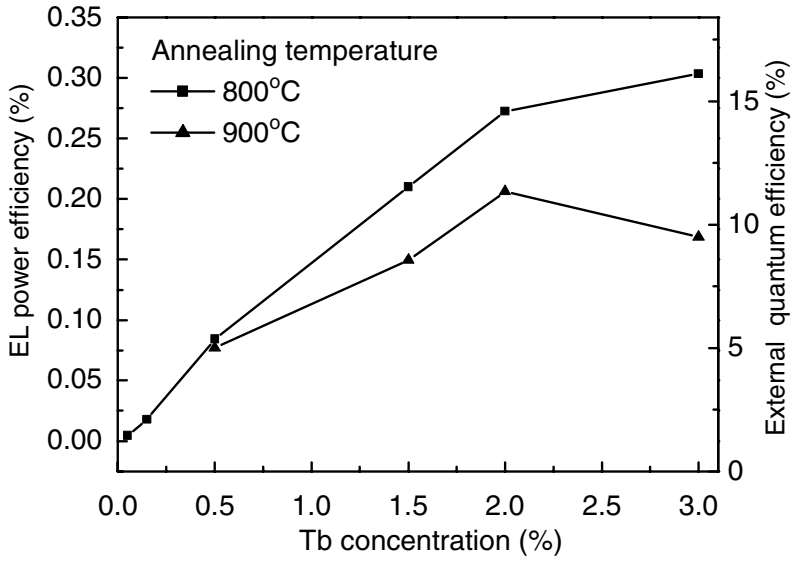

Figure 4. Variation of the EL power efficiency and the external quantum efficiency with Tb concentration at a current of 10 μA for a device size of 0.5 mm in diameter. The annealing was done at 800°C and 900°C.

Tb concentration

Fig.5 (a) compares the concentration dependence of the EL peak intensity from $^5D_3$-$^7F_5$ (blue peak at 413 nm) and $^5D_4$-$^7F_5$ (green peak at 541 nm) for the samples annealed at 800°C for 1 hour. The EL intensity is measured at a constant current injection of 10 μA. The green peak increases linearly with increasing Tb concentration up to 2% and then saturates while the blue peak shows strong concentration quenching after increasing the Tb concentration above 0.15 %. Fig.5 (b) shows the peak intensity ratio of the blue divided by the green peak (B/G ratio) as a function of Tb concentration. The B/G ratio decreases with increasing Tb concentration, which indicates a more effective population of the $^5D_4$ levels. To trace back the origin of this behavior, we have measured the EL decay time of the blue ($^5D_3$) and green ($^5D_4$) lines as seen in Fig. 5c. The decay time of the $^5D_3$ level decreases with increasing Tb concentration while the decay time of the $^5D_4$ level slightly increases. This indicates a faster non-radiative decay of $^5D_3$ leading to a higher average population of $^5D_4$. We attribute this behavior to the cross-relaxation from the $^5D_3$ to the $^5D_4$ level in adjacent Tb3+ ions, made possible through the very small energy mismatch of 11 meV for ($^5D_3$-$^5D_4$)≅($^7F_0$-$^7F_6$). Such a cross-relaxation results in an increase of the transitions from $^5D_4$ to the ^7F_j (j=3-6) levels as compared to the strong quenching of the $^5D_3$ to ^7F_j (j=3-6) peaks in the EL spectra. Therefore, efficient green EL is obtained at a higher Tb content.

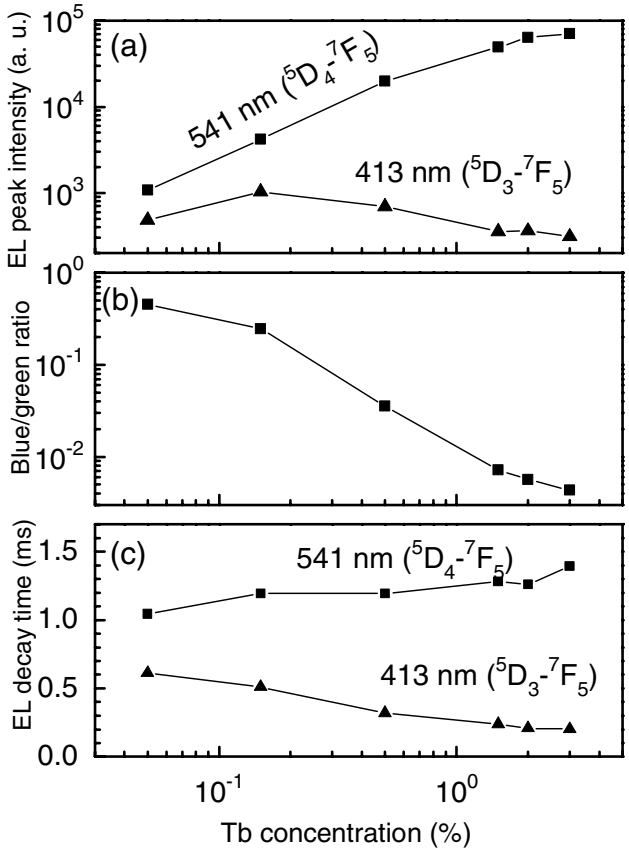

Figure 5. Concentration dependency of the EL intensity **(a)**, the blue/green ratio (B/G ratio) **(b)**, and the lifetime **(c)** of the two transitions from $^5D_3$-$^7F_5$ (blue peak at 413 nm) and $^5D_4$-$^7F_5$ (green peak at 541 nm). The annealing was done at 800°C for 1 hour. The EL intensity was measured at a constant current injection of 10 μA.

EL excitation mechanism

The EL from rare earth ions present in a matrix under high electric field can be excited via two processes. One is the direct impact excitation by energetic hot electrons into the conduction band of the matrix. The charge states of the rare earth ions do not change during the excitation process. The other process is the excitation across the SiO_2 band gap or of defects, and the subsequent energy transfer to the RE ions. In the former process, the relative intensity of the peaks from higher excited levels normally increases faster than those at lower energy levels due to an increase in the average energy of the hot electrons with increasing electric field. In the latter, since the excitation comes from the energy transfer, the relative intensity of the emission peaks of rare-earth ions is mainly controlled by the thermal equilibrium between different energy levels of the rare earth ions. Therefore, the relative intensity of the different peaks will not change dramatically with increasing electric field.

From an analysis of the B/G ratio vs. the electric field an increase of that ratio was observed. This gives strong evidence that the EL excitation is dominated by direct impact excitation of the hot electrons in the conduction bands of SiO_2 by F-N tunneling (see above). Moreover, a strong decrease in the B/G ratio with increasing Tb concentration was observed. This proves that the cross-relaxation from the higher excitation level $^5D_3$ to $^5D_4$ is also involved in the excitation of the lower lying $^5D_4$ level. Therefore, the peaks of $^5D_4$-^7F_j (j=3-6) transitions were excited by both the impact excitation and the cross-relaxation from $^5D_3$ states at high Tb concentration. The above excitation mechanism explains the change of EL spectra with Tb concentration and annealing temperature in Tb-doped SiO_2 MOSLEDs. It also explains the correlation between the onset of the EL and the strong F-N tunneling injection of hot electrons as shown in Fig.4. For more details and description of the EL excitation cross section, see Ref. 5.

LUMINESCENCE AND CHARGE TRAPPING IN MOSLEDs WITH (Er,Si) RICH SiO_2

For many years Er implanted SiO_2 films have attracted considerable interest due to the possibility of making EL devices that operate at a wavelength of 1.54 μm, i.e. within the range of optical transparency of quartz optical fibers. Critical issues of the device performance are the relatively low emission efficiencies and the low currents that can be passed through the dielectric. It has been shown in a number of studies that the introduction of Si nanocrystals into Er-doped SiO_2 enables the intensity of the PL at 1.54 μm to be largely increased while causing concurrently a somewhat reduced EL intensity. However, the mechanism of attenuation of the Er associated EL at 1.54 μm after introducing Si nanoclusters into the SiO_2 matrix has not been elucidated. Our recent work provides new insights into the relationship between light emission efficiency and charge trapping in Er doped SiO_2 containing Si nanoclusters. The influence of the Si nanocluster density on both the capture of charge carriers at traps associated with the presence of Er and the resulting PL and EL at 1.54 μm was examined, for more details see Ref.[7].

Si wafers with a 200 nm thick thermally grown SiO_2 film were used to produce the MOSLEDs. Si^+ ions were implanted at two energies of 35 and 80 keV, which generated a fairly flat-topped profile of 1.1 to 15 at. % excess silicon atoms over a depth region of 65 to 150 nm. After annealing at 1100°C in an N_2 ambient for 1 h necessary to form Si nanocrystals, Er^+ ions were implanted at 280 keV with a dose of 1×10^{15} cm^{-2} in such a way as to position the peak of their distribution in the central part of the Si cluster profile. Finally, the samples were annealed at 850°C in an ambient of N_2 for 30 min to reduce the amount of the implantation induced damage

and activate the implanted Er^{3+} centers. The top electrodes were 100 nm indium-tin-oxide (ITO) layers patterned into circular dots with a diameter of 0.05 to 1.00 mm.

The formation of Si nanoclusters and Er^{3+} centers was monitored by PL measurements over the wavelength range of 600 to 900 nm and at 1535 nm using the 532 nm line of a Nd:YAG laser and the 633 nm line of a He-Ne laser with a power of 5 mW as the excitation sources, respectively. Measurements of the EL and charge trapping were carried out in a high field, constant current injection regime. Charge traps were studied over a wide range of cross sections using three levels of injected constant current density, namely 1×10^{-7}, 2×10^{-5} and 5×10^{-4} A cm^{-2}, with the last value of the current density being typical of the regime of EL excitation. During the current injection, negative (or positive) charges were trapped within the oxide layer, which caused a decrease (or increase) in the electric field gradient at the Si/SiO_2 interface. In order to maintain a constant current injection, one needs to shift the applied voltage as the trapped charges change. Charge trapping processes were studied under conditions of electron injection from the Si substrate into the oxide by measuring the shift of the applied voltage with the injected charge Q_{inj}. The absolute value of the net trapped charge was calibrated using the shift of the flat band voltage, ΔV_{FB}, extracted from the high frequency (1 MHz) capacitance-voltage (C-V) characteristics after injecting an electron charge of 1×10^{13} e cm^{-2}.

Fig. 6 (a) shows EL spectra measured over the wavelength range of 1450 to 1650 nm in Er implanted structures containing Si nanocrystals of different density. The peak at 1535 nm, which is characteristic of the intra-transition of the electron in the Er^{+3} ion from the excited $^4I_{15/2}$ state to the ground state, is clearly seen. A broad PL peak centered at 700 nm was observed as a result of the introduction into the oxide of an excess of Si atoms above 3 at %. The position of the PL peak did not change with increasing Si concentration. The relative PL intensity of the emission peak of the Si nanocrystals and the peak at 1535 nm due to the presence of Er^{3+} ions are shown in Fig.1(b). One can see that the increase in Si nanocluster density results in an

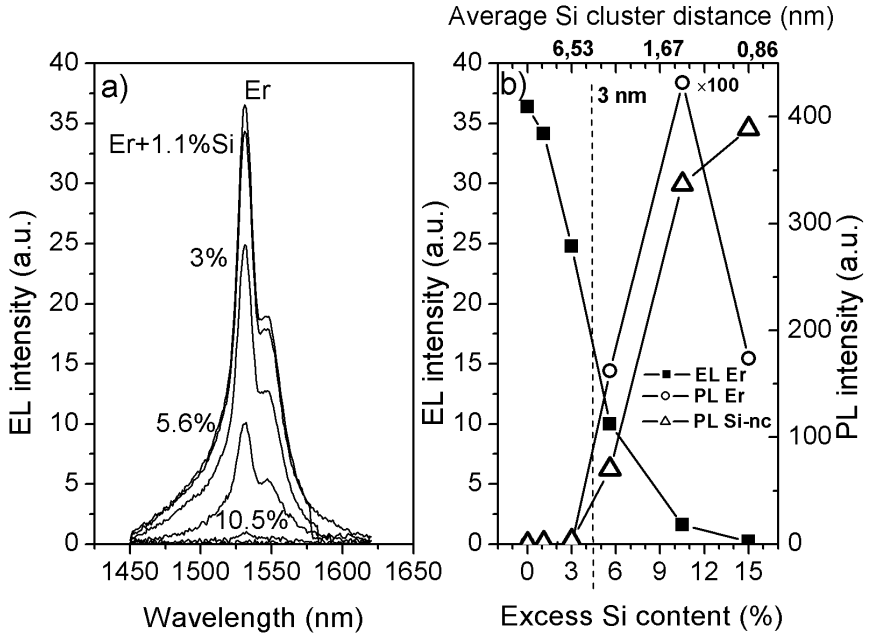

Figure 6. (a) Electroluminescence (EL) spectra of the ITO-SiO_2-Si structures with SiO_2 containing Si nanoclusters and Er , and **(b)** PL and EL intensity at 1535 nm wavelength and PL intensity at 707 nm wavelength in dependence on excess Si content.

increased PL intensity of the infrared peak from Er^{3+}. A maximum value is observed at an excess Si content of 10 at %. In contrast, the EL intensity at 1535 nm is strongly quenched for such an excess silicon concentration. It should be noted that the intensity of the infrared EL diminishes strongly with decreasing average distance between the silicon clusters below the mean free path of the hot electrons (or heat up distance), which equals to approximately 3 nm. Our calculations show that for Si nanoclusters with a mean size of 3 nm, the average distance between the nanoclusters becomes smaller than 3 nm for an excess Si content of more than 5 at. % (see Fig.6(b)). Thus, the average energy of the electrons will decrease with increasing the fraction of direct tunneling among the silicon nanoclusters.

It should also be noted that in our case EL from Si nanoclusters has not been observed at the currents and voltages used, up to the breakdown of the dielectric. This can serve as evidence of the ineffective excitation of the Si nanoclusters by the high-energy injected electrons. Due to the inefficient excitation of silicon nanoclusters, the EL from the Er centers cannot be excited efficiently through the strong energy transfer from the excited silicon clusters to the Er centers compared with the PL excitation processes.

The analysis of the current-voltage characteristics revealed that up to a 3 at % excess Si content the current injection through the dielectric can be described by the Fowler-Nordheim electron tunneling mechanism. For a higher concentration of the excess Si atoms of 5.6 at.%, the effective potential barrier for FN tunneling decreases from 3.15 to 2.90 eV. This points to the influence of trapping on the electron tunneling through the triangular potential barrier from Si to the SiO_2 conduction band, the so-called trap-assisted tunneling mechanism. At a higher excess Si content there is a transition from FN tunneling to direct tunneling between silicon clusters.

The dependence of the trapped charge on the injected electron charge is shown in Fig. 7. The starting unimplanted oxide exhibits practically no charge trapping following electron injection at a charge density of 10^{13} e cm^{-2}. After the same level of injection the Er^{+} implanted sample shows considerable positive charge trapping. This indicates the presence of hole traps with a giant cross section ($\sigma_{h0} > 10^{-13}$ cm^2) in the Er-implanted oxide. The subsequent introduction into the Er-implanted oxide of Si nanoclusters results in additional electron trapping and points towards the formation of negative charge traps with a giant cross section ($\sigma_{e0} > 10^{-13}$ cm^2). Furthermore, an increase in the Si nanoclusters density up to 15 % is accompanied by an increased magnitude of the trapped negative charges (see inset to Fig. 7).

The most important findings from data processing of the charge carrier trapping (details in [8,9]) may be summarized as follows. The starting structure exhibits only hole traps with cross sections $\sigma_{h1} \approx 6.2\times10^{-15}$ cm^2, $\sigma_{h2} \approx 1.2\times10^{-15}$ cm^2 and $\sigma_{h3} \approx 4.7\times10^{-17}$ cm^2. The implantation of Er, apart from hole traps of a giant cross section ($>10^{-13}$ cm^2), introduces into the oxide an appreciable concentration of electron traps of a large cross section $\sigma_{e1} \approx 7.0\times10^{-14}$ cm^2 and $\sigma_{e2} \approx 7.0\times10^{-15}$ cm^2 as well as a specific pair of electron and hole traps with similar cross sections $\sigma_e^{Er} \approx 3.0\times10^{-18}$ cm^2 and $\sigma_h^{Er} \approx 6.0\times10^{-18}$ cm^2, respectively. The additional implantation of Si, resulting in the formation of Si nanoclusters, apart from creating electron traps of a giant cross section, increases too the concentration of electron traps with the following cross sections: $\sigma_{e1}\approx7\text{x}10^{-14}$ cm^2, $\sigma_{e2}\approx7\text{x}10^{-15}$ cm^2 and $\sigma_{e3}\approx1.5\text{x}10^{-15}$ cm^2. However, as the concentration of the extra Si exceeds 5.6 at.%, the capture of electrons at these traps shows a dramatic decrease. For excess Si concentrations above 3 at. %, there is also a considerable reduction in the charge trapping at the electron/hole trap pair of a small cross section ($\sim10^{-18}$ cm^2) that is formed following the implantation of Er.

Thus, it is believed that large Er inclusions, which trap effectively positive charge, create

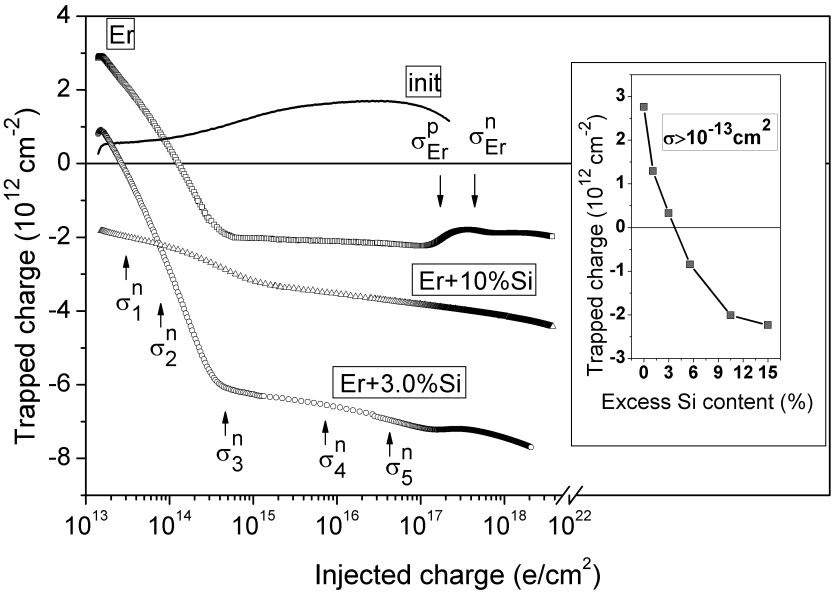

Figure 7: Net trapped charge calculated from the change in voltage applied to the MOSLED in a constant current regime as a function of injection charge from the Si substrate, for Er and Si implanted SiO_2. Inset: Charge on the traps with capture cross-section of more than 10^{-13} cm^2 as a function of excess Si content.

in their vicinity defects that can capture electrons. The introduction of Si nanocrystals into the matrix enhances the process of electron trapping at these crystallites as well as in the presumably disordered surroundings, which may lead to Coulomb scattering of the injected electrons and attenuation of their interaction with the Er centers around them. Since the excitation of the Er through the excitation of the Si clusters is not efficient in the EL process, we suggest that Er excitation is mainly due to direct impact excitation of hot electrons, which are accelerated by the high electric field in the SiO_2 conduction band after FN tunneling injection from the Si substrate. The scattering of hot electrons by both the charged defects and the Si nanoclusters results in a reduction of the average energy and the average impact excitation cross section of the Er centers around the negatively charged nanoclusters. Increasing the Si nanocrystal density (for excess Si concentrations larger than 5 at. %) alters the conductance from FN tunneling to direct tunnelling through silicon clusters. The tunnelling electrons have insufficient energy to excite Er centers, which subsequently reduces the EL efficiency.

The defect influence on the product of the effective electron life time (τ) and the effective cross section of excitation (σ) can be estimated from the dependence of the EL intensity on current density. The value $\sigma\tau$ decreases about seven times with increasing excess Si content from 1.1 to 15 at.%. In a study [10] of the dependence of the Er luminescence decay time on the excess Si concentration from 2.4 to 11% after annealing at the same temperature of 1100^{o}C, the lifetime of the Er-induced PL was found to decrease only by a factor of about 2 (from 4.4 to 2.1 ms). This means that the excitation cross section of Er was reduced by a factor of more than 3 in the EL excitation by introducing Si clusters with an excess Si content of up to 15 %.

Such different behavior of the PL and EL depending on the Si nanocrystals density is associated primarily with the different nature of the excitation in the vicinity of the Er^{3+} ion. In the PL excitation process, the excitation of Er occurs via naturally charged exciton relaxation created in the Si nanoclusters, which does not alter significantly the electric field around the Si

nanocrystals. In the EL excitation process, electrons trapped at the Si nanoclusters act repulsively to the hot electrons for excitation of both of the nanoclusters and the Er centers in the surroundings. This could be one of the reasons for the insufficient excitation of both the EL from nanoclusters and the Er centers with introducing discrete Si clusters. The larger the number of the Si nanocrystals surrounding an Er inclusion, the more efficient screening of the electric field among the clusters occurs, which is essential for the heating of electrons. Consequently, in considering the excitation of Er ions by electrons passing through an amorphous SiO_2 layer, one should take into account their interaction with the defect environment of the Er inclusions.

APPLICATION ASPECTS

The most attractive applications for MOSLEDs are those utilizing the main advantages of these light emitters. As all processing steps are standard procedures of common Si technology, the manufacturing of the MOSLED is inexpensive and very interesting for disposable products. Furthermore, the size and the shape of the light emitters are only limited by lithography patterning allowing the design of versatile application-specific layouts. To demonstrate the ability to manufacture miniaturized light sources, MOSLEDs with a feature size down to 4 µm were successfully implemented [11]. Based on this, the MOSLED is especially suitable for use in biochips tracing specific substances with fluorescence analysis. In a standard test procedure, the biochip consists of an array of sample spots with either variably prepared surfaces to test one sample for different substances or with uniformly prepared surfaces to test a set of different samples. The substance under investigation is labeled with a dye normally excited by a laser. An optical system guides the laser light to the sample. In order to get a spatial resolution, either a mechanical scan over the array has to be performed or a CCD camera has to be used (Fig. 8, left). In the latter case, the light signal splits into a large number of pixels complicating the detection of low light intensities. Generally, an edge filter in front of the detection system is placed in order to separate the laser light from the emission of the dye. If an array of MOSLEDs

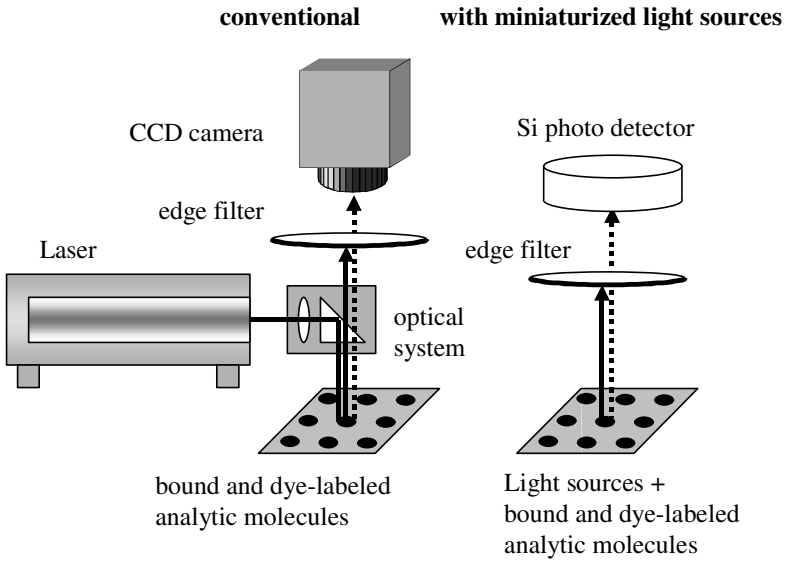

Figure 8. Schematic illustrating the fluorescence analysis on a biochip using the conventional route (left) and the advanced route with miniaturized MOSLEDs (right).

with a suitable emission wavelength is used, the laser and the corresponding optical system is no longer needed (Fig. 8, right). As each of the MOSLEDs can be turned on and off individually, the spatial resolution is already given by the mode of electrical excitation. It is sufficient to record the light of the dye with a high-quality, large-area but inexpensive Si detector. As the detector records an integral signal, much weaker light intensities can be detected. As a result, the fluorescence analysis can be performed with a technical setup considerably shrunk in size, which is very suitable for point-of-care diagnostics.

CONCLUSIONS

RE based MOSLEDs show promising electroluminescence performance. This is based on a purpose-designed MOS capacitor optimized for maximum power efficiency. New light is shed onto the understanding of the correlation between optical and electrical properties of silicon dioxide based light emission structures.

ACKNOWLEDGEMENTS

Stimulating discussions and experimental support with/by V.S. Lysenko, I.P. Tyagulskii and J. Vovk at NASU Kyiv, and R.A. Yankov at FZR are kindly acknowledged. We are thankful to the Rossendorf Implantation Group as well as the Semiconductor Processing Group for their careful processing work. The Bundesministerium für Bildung und Forschung supported part of the work within the WTZ Program.

REFERENCES

[1] L. Pavesi, S. Gaponenko, and L. Dal Negro,(eds) “Towards the First Silicon Laser” Proc. NATO Adv. Research Workshop, Trento Sept. 21-26, 2002, (Kluwer Acad. Publ. 2003).
[2] W. Skorupa, L. Rebohle, T. Gebel, and M. Helm, in [1], p.69, and Appl.Phys. **A76**, 1049 (2003).
[3] L. Rebohle, J. von Borany, D. Borchert, H. Fröb, T. Gebel, M. Helm, W. Möller, and W. Skorupa: J. Electrochem. Soc.: Electrochem. and Solid State Lett. **7**, G57 (2001).
[4] J.M. Sun, W. Skorupa, T. Dekorsy, M. Helm, L. Rebohle, and T. Gebel Appl. Phys. Lett. **85**, 3387 (2004).
[5] J.M. Sun, W. Skorupa, T. Dekorsy, M. Helm, L. Rebohle, and T. Gebel J. Appl. Phys. (2005) submitted.
[6] S. Nagahama, et al., Phys. Stat. Sol. (a) **188**, 1 (2001).
[7] A.N. Nazarov, J.M. Sun, W. Skorupa, R.A. Yankov, I. N. Osiyuk, I. P. Tjagulskii, V. S. Lysenko, and T.Gebel., Appl. Phys. Lett. **86**, 151914 (2005).
[8] A.N. Nazarov, T. Gebel, L. Rebohle, W. Skorupa, I.N. Osiyuk and V.S. Lysenko, J.Appl.Phys. **94**, 4440 (2003).
[9] A.N. Nazarov,W. Skorupa, I.N. Osiyuk, I.P. Tjagulskii, V.S. Lysenko, R.A. Yankov and T. Gebel, J. Electrochem. Soc. **152**, F20 (2005)
[10] M. Fujii, K. Imakita, K. Watanabe, and S. Hayashi, J.Appl.Phys. **95**, 272 (2004).
[11] L. Rebohle, T. Gebel, R.A. Yankov, T. Trautmann, W. Skorupa, J. Sun, G. Gauglitz, and R. Frank, Optical Materials **27**, 1055 (2005)